INTERNATIONAL JOURNAL OF HYDROGEN ENERGY XXX (2015) 1–11

Available online at www.sciencedirect.com

ScienceDirect

journal homepage: www.elsevier.com/locate/he

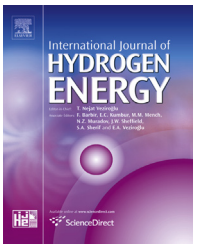

Hydrogen cycling properties of xMg–Fe materials (x: 2, 3 and 15) produced by reactive ball milling

J.A. Puszkiel[*], *P. Arneodo Larochette*, *A. Baruj*, *G. Meyer*, *F.C. Gennari*

Instituto Balseiro (UNCuyo and CNEA) and Consejo Nacional de Investigaciones Científicas y Técnicas (CONICET), Centro Atómico Bariloche, Av. Bustillo km 9.5, R8402AGP, S. C. de Bariloche 8400, Argentina

ARTICLE INFO

Article history:
Received 2 September 2015
Received in revised form
27 October 2015
Accepted 28 October 2015
Available online xxx

Keywords:
Cycling
Hydrides
Magnesium hydride
Microstructure
Kinetics

ABSTRACT

This work deals with the hydrogen cycling properties of xMg-Fe (x: 2, 3 and 15) elemental powder mixtures produced via low energy ball milling under hydrogen atmosphere at room temperature. The cycling process is carried out at constant temperature of 375 °C in a closed loop device. The evolution of both hydrogen storage capacity and absorption kinetic behavior are monitored during pressure cycling. Changes induced by cycling are characterized via scanning electron microscopy (SEM), differential scanning calorimetry (DSC), X-ray diffraction (XRD) and particle size distribution (PSD). All studied materials lost part of their hydrogen storage capacity during hydrogen cycling. This capacity reduction results from a combination of two effects: Mg evaporation and the formation of Mg_2FeH_6 which is stable at the experimental conditions. While the hydrogenation rates are not affected, the dehydrogenation kinetic properties of the materials are influenced by the cycling process.

Introduction

Several studies have shown that Mg–Fe mixtures exhibit better hydrogen absorption–desorption properties than pure Mg [1–19]. Many of these works studied the catalytic effect of Fe on the hydrogen absorption–desorption properties of MgH_2 [1–8], while others investigated the hydrogen storage properties of the MgH_2–Mg_2FeH_6 hydride mixture [9–19]. The Mg–Fe–H hydride system is interesting from the technological standpoint due to the low cost of Mg and Fe and its potential hydrogen and energy storage properties, i.e. fast intrinsic absorption – desorption rates (3–5 min at 300 °C–350 °C) [8], relative high hydrogen capacity (5.4 wt.% H for Mg_2FeH_6 and 7.6 wt.% H for MgH_2) and high heat storage capacities (energy to weight: 1817 kJ/kg for Mg_2FeH_6 and 1837 kJ/kg for MgH_2) [20–22]. It has been reported that, even under conditions where almost no complex hydride is formed, the presence of Fe has a strong effect on improving the hydrogen hydrogenation–dehydrogenation kinetics of Mg. For example, the mixture 15Mg–Fe has a faster kinetic response than pure Mg and higher storage capacity than the 2Mg–Fe composition [8].

Technological applications of hydride forming materials usually entail a large number of hydrogen absorption–desorption cycles. For this reason, a complete characterization of hydrogen storage materials should include the evaluation of their properties under cycling conditions. There are few reports in the literature about the cycling behavior of Mg–Fe–H system when both hydride phases (Mg_2FeH_6–MgH_2) are present [20–22]. Reiser et al. [20] have found that the hydrogen storage capacity remains unchanged for both MgH_2

* *Corresponding author*. Tel.: +54 294 4445118/97; fax: +54 294 4445190.
E-mail address: julianpuszkiel1979@gmail.com (J.A. Puszkiel).
http://dx.doi.org/10.1016/j.ijhydene.2015.10.140

(starting from pure Mg or 4:1 and 20:1 of Mg:Fe mixtures) and Mg_2FeH_6 (starting from a 2Mg–Fe mixture). Bogdanović et al. [21, 22] have performed experiments with several Mg–Fe compositions. In the case of the Mg_2FeH_6 complex hydride, its hydrogen capacity remained constant at 5 wt. % H during 600 absorption–desorption cycles performed above 500 °C and 180 min each cycle. It has been concluded that the separation of Mg and Fe in two immiscible phases upon dehydrogenation and the formation of the complex hydride phase upon hydrogenation counteracts the agglomeration and it is one of the causes of the cycling stability. All the above described investigations [20–22] have been performed at severe absorption and desorption conditions (high temperatures: above 500 °C, for long absorption and desorption times: several hours and under high hydrogen pressures: around 100 bar), aiming to evaluate the cycling stability of the Mg–Fe complex hydride [21]. There are some works [23–25] about the cycling stability of Mg-based films containing Al, Fe, Ti and about ternary systems such as Mg–Fe–V, Mg–Al–Ti, Mg–Fe–Ti and Mg–Al–Fe studied at temperatures around 200 °C and pressures below 5 bar during 100 cycles. It was found that mainly Mg–Al–Ti and Mg–Fe–Ti are relatively stable against cycling and can intake 4–6 wt. % H. Additionally, the $Mg_{10}Fe_{30}$ material tested at such low temperature absorbed 4.8 wt % H during the first cycle due to the formation of Mg_2FeH_6 and smaller amounts of MgH_2. However, the material just absorbed 0.6–0.8 wt. % H in subsequent cycles. This low cycling stability was attributed to the tiny amount of reversible MgH_2 and the higher stability of Mg_2FeH_6 that formed under the experimental conditions.

As described above, the cycling stability of the Mg–Fe–H system was tested either under very high temperature and pressure conditions or under extremely low temperature and pressure conditions [20–25]. These combinations of pressure and temperature conditions are quite far from the conditions found in most of the practical applications. On one hand, the severe temperature and pressure conditions require exceptional mechanical properties for the reservoir's material at the time to build a tank. On the other hand, when Mg–Fe–H system is used at too low temperatures there is a limited reversible hydrogen storage capacity. The cycling stability behavior of the Mg–Fe–H system over a wide range of Mg–Fe compositions and under moderate temperature (<400 °C) and pressure (less than 40 bar for hydrogenation and more than 2 bar for dehydrogenation) has not been yet investigated. These moderate conditions would be closer to those found in possible practical applications, i.e. not too demanding for the vessel's material and where the hydride still retains a high reversible hydrogen capacity.

In this work, we studied the behavior of xMg–Fe materials (x: 2, 3, 15) subjected up to 1000 successive hydrogen absorption–desorption cycles at 375 °C in a closed loop device. The materials selection allows studying the cycling properties of the stoichiometric mixture leading to the formation of Mg–Fe complex hydride and the properties of Fe-catalyzed Mg [8]. All investigated materials were synthesized via reactive mechanical milling under hydrogen atmosphere (RMM). The effects of cycling on the absorption capacity and the influence on the hydrogenation–dehydrogenation characteristics were investigated via X-ray diffraction, calorimetry, particle/agglomerate size distribution and volumetric techniques.

Experimental

Synthesis

Mg–Fe elemental powder mixtures (Mg purchased in Riedel-de Haën – purity: 99.9%; Fe purchased in Sigma Aldrich – purity: 99.9%) with three different compositions, namely 2Mg–Fe, 3Mg–Fe and 15Mg–Fe, were prepared via low energy reactive mechanical milling (RMM) at 5 bar of H_2 and during 150–200 h as explained in Ref. [8].

The prepared samples are hereafter referred to as 2Mg–Fe, 3Mg–Fe and 15Mg–Fe. All handling was carried out in Plas-Labs and MBraun Unilab glove boxes with controlled H_2O and O_2 atmosphere to minimize the oxidation/hydrolysis of the samples.

Cycling behavior

The prepared Mg–Fe mixtures were subjected up to 1000 hydrogen absorption/desorption cycles at a constant temperature of 375 °C in a closed loop device. For all materials, 200–300 mg of mass was used to evaluate their cycling performance. The samples were weighted in the hydrogenated condition before and after the experiments in order to detect and quantify possible mass loss due to cycling. The closed loop device was designed to study intrinsic pressure cycling degradation of hydride forming materials [26]. The device uses a hydride forming material ($LaNi_5$) as a hydrogen source/sink. Prior to each absorption cycle, hydrogen was released from the source to fill an intermediate volume up to a pre-established pressure. This volume was then isolated from the source and connected to the sample reactor. A filling pressure in the intermediate volume was calculated in order to get an initial pressure in the sample reactor of 3000 kPa after connecting both volumes. After the initial pressure drop owing to the connection of the intermediate and sample reactor volumes, a traditional Sieverts measurement was performed (absorption started at 3000 kPa and finished above 2500 kPa). The final absorption pressure was far higher than the Mg–Fe–H equilibrium pressures at 375 °C, i.e. $P_{eq.(375°C)}$ is between 1000 and 1400 kPa [8]. The pressure drop caused by the hydrogen absorption in the sample was monitored as a function of time. For the desorption stage, the source/sink was first cooled in order to reduce its equilibrium pressure down to a desired value (300 kPa). All the volumes were then connected (sample reactor, intermediate volume and hydrogen source/sink) causing the sample dehydrogenation and the source/sink hydrogenation simultaneously. The dehydrogenation of the sample started at 300 kPa and finished at a lower value of about 250 kPa because of source/sink continuous hydrogenation. This dehydrogenation procedure did not allow to quantify the storage capacity and to measure the reaction rate during the desorption stages. The range of pressure used for the dehydrogenation process (from 300 kPa to 250 kPa) was much lower than the decomposition equilibrium pressures for MgH_2 at 375 °C, i.e. $P_{eq.(375°C)}$ is about 1000 kPa [8]. However, the range of

Please cite this article in press as: Puszkiel JA, et al., Hydrogen cycling properties of xMg–Fe materials (x: 2, 3 and 15) produced by reactive ball milling, International Journal of Hydrogen Energy (2015), http://dx.doi.org/10.1016/j.ijhydene.2015.10.140

pressure used was not so far away from the decomposition equilibrium pressures of Mg_2FeH_6 at 375 °C, i.e. $P_{eq.(375°C)}$ about 500 kPa [8]. The time elapsed between two consecutive absorption stages was approximately 15 min. After each hydrogenation and dehydrogenation cycle, the storage capacity of the sample was recorded. In order to determine the evolution of the reaction kinetics, detailed pressure drop measurements were conducted every five cycles using absorption/desorption intervals two times longer than during regular cycles (so called: detailed cycles). The evolution of the hydrogen capacity as a function of the number of cycles was plotted using the measured hydrogen capacities corresponding to the hydrogenation processes after the detailed cycles. These points were selected in order to measure the hydrogenation processes with a sample as fully dehydrogenated as possible, so that the storage capacity can be accurately measured.

Characterization and kinetic behavior

The samples before and after cycling were characterized by different techniques in order to identify possible changes induced by the process. Phase identification, microstructural properties and relative phase composition of the materials were investigated by XRD (Philips Instruments PW 1710/01) using CuK_α radiation ($\lambda = 1.5405$ Å, graphite monochromator, 30 mA and 40 kV). The crystallite size of the hydride phases was determined by the Scherrer equation [27]. In order to calculate the ratio between the relative amounts of the hydride phases (amount of MgH_2 to Mg_2FeH_6), the K value method with the integrated intensities of the strongest XRD peaks was used. This method is based on the following equations:

$$\frac{I_{MgH_2}}{I_{Mg_2FeH_6}} = K_{MgH_2/Mg_2FeH_6} \times \left[\frac{X_{MgH_2}}{X_{Mg_2FeH_6}}\right] \quad (1)$$

$$X_{MgH_2} + X_{Mg_2FeH_6} = 1 \quad (2)$$

where I_{MgH_2} and $I_{Mg_2FeH_6}$ are the integrated intensities of the strongest XRD peaks 2θ: 27.9°, referring to [110] for MgH_2 and 24.1°, referring to [111] for Mg_2FeH_6; K_{MgH_2/Mg_2FeH_6} is a constant and X_{MgH_2} and $X_{Mg_2FeH_6}$ are the relative abundances of the hydride phases. This method is indeed applicable to a mixture containing two phases. However, in this case it was utilized to estimate the relative amounts of hydride phases in a mixture containing more than two phases [28].

Morphological and agglomerate size distribution analyses of the samples were performed by scanning electron microscopy (SEM 515, Philips Electronic Instruments). The powder samples were dispersed in stickers and observed with secondary electrons. Moreover, the agglomerate size distributions (so called PSD) of the cycled powder materials were determined by using a Mastersizer Micro MAF 5000 device with a measurement range between 0.3 μm and 300 μm. The samples were first diluted in n-butanol, then stirred at 2100 rpm and subsequently measured.

Thermal desorption behavior of the hydride phases was studied by differential scanning calorimetry (DSC, TA 2910 calorimeter), using heating rates of 1 °C/min, 2 °C/min, 5 °C/min, 10 °C/min, 15 °C/min and 25 °C/min and argon flow rate of 122 ml/min. The desorption capacities and the relative weight percentages of the phases in the samples were determined from the area of the DSC curves and the stoichiometry of the Mg–Fe starting materials without taking into account the formed amount of MgO or $Mg(OH)_2$.

The mechanism for the hydrogenation process was analyzed with the Johnson, Mehl and Avrami (JMA) gas–solid reaction model based on nucleation and growth of transformations in metals and alloys [29]. This model describes the reaction in terms of the following equation:

$$f = 1 - \exp\left[-(k.t)^n\right] \quad (3)$$

Here, f is the transformed fraction, k the rate constant, t is time and n is the so-called Avrami exponent which depends on the controlling step mechanism ($m = 1$ for interface controlled growth and $m = 2$ for diffusion controlled growth) and dimensionality growth ($d = 1$, 2 and 3 for 1D, 2D and 3D growth, respectively). Thus, the exponent n can be expressed as:

$$n = \frac{d}{m} + 1 \quad \text{for constant nucleation rate} \quad (4)$$

$$n = \frac{d}{m} \quad \text{for constant nuclei number} \quad (5)$$

The JMA equation was fitted to the hydrogenation curves at the first cycle and then every 100 cycles. The fittings were performed from $f = 0$ to $f = 0.8$. The hydrogenation rate at $f = 0.5$ obtained from each fitted expression was plotted as against the number of cycles to assess the sorption kinetic behavior through cycling.

In order to investigate the effect of the hydrogen cycling upon the dehydrogenation behavior, the activation energy was calculated by the Kissinger method based on the following equation [30]:

$$\ln\left[\frac{\beta}{T_m^2}\right] = -\frac{E_a}{RT_m} + \ln\left[\frac{AR}{E_a}\right] + C \quad (6)$$

where β is the value of the heating rate (when expressed in K/min), T_m is the absolute temperature of the DSC peak maximum, R is the ideal gas constant, A is the pre-exponential factor, E_a is the activation energy and C is a constant.

Results

Cycling behavior xMg–Fe (x = 2, 3 and 15) materials

Milling in hydrogen atmosphere is a one-step synthesis method which involves the in-situ formation of hydride phases facilitated by the microstructure refinement of the materials during the process. Hence, via reactive mechanical milling (RMM) materials with improved hydrogen sorption characteristics can be obtained [4,7,31]. Fig. 1 shows the results of hydrogen cycling experiments at 375 °C for xMg–Fe (x: 2, 3 and 15) samples. The 15Mg–Fe material has the highest storage capacity throughout cycling (Fig. 1(a)). Its storage capacity sharply drops during the first 40 cycles, then suffers a kind of activation and finally decreases steadily. In the case of 3Mg–Fe (Fig. 1b), the material does not show an initial stage like the 15Mg–Fe. At the beginning and end of the cycling

Please cite this article in press as: Puszkiel JA, et al., Hydrogen cycling properties of xMg–Fe materials (x: 2, 3 and 15) produced by reactive ball milling, International Journal of Hydrogen Energy (2015), http://dx.doi.org/10.1016/j.ijhydene.2015.10.140

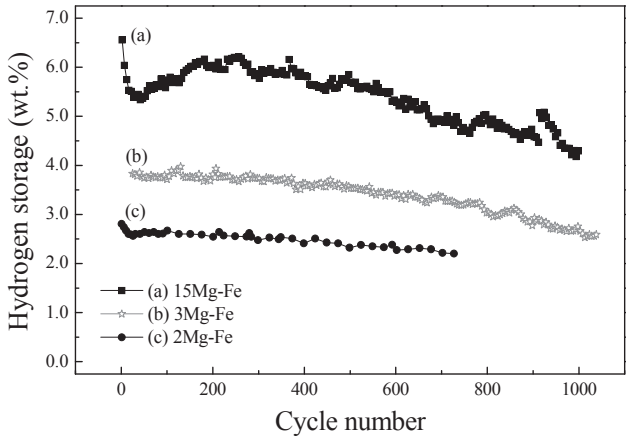

Fig. 1 – Evolution of the hydrogen storage capacity throughout the hydrogenation–dehydrogenation cycles at 375 °C for: (a) 15Mg–Fe, (b) 3Mg–Fe, (c) 2Mg–Fe.

process, it has a hydrogen capacity higher than the 2Mg–Fe (Fig. 1(c)). However, its storage capacity progressively falls during cycling.

Characterization of the xMg–Fe (x = 2, 3 and 15) materials

The xMg–Fe materials before and after cycling were characterized by XRD, DSC, SEM and PSD. Figs. 2 and 3 show the XRD–DSC and SEM characterizations, respectively and Table 1 summarizes the main characteristics of the xMg–Fe (x: 2, 3 and 15) materials before and after cycling.

The XRD and DSC results of the 2Mg–Fe before and after cycling are shown in Fig. 2A and B, respectively. After RMM (Fig. 2A(a)), the XRD pattern shows Fe, MgH_2 and Mg_2FeH_6 reflections. The observed MgH_2 and Mg_2FeH_6 broad peaks account for the small crystallite sizes reached after the RMM process [8,31]. After cycling (Fig. 2A(b)), all XRD peaks are narrower due to crystallization by cycling at relative high temperatures. The presence of Mg_2FeH_6, MgH_2, Fe, Mg and MgO is detected. The DSC curves shown in Fig. 2B correspond to a heating rate of 5 °C/min. The non-cycled sample (Fig. 2B(a)) exhibits a shoulder at about 220 °C and a peak maximum at about 260 °C. This behavior is related to overlapped endothermic events associated to the decomposition of MgH_2 (first peak maximum) and Mg_2FeH_6 (second peak maximum) [19]. On the other hand, the DSC curve corresponding to cycled 2Mg–Fe (Fig. 2B(b)) only shows a single thermal event with a peak maximum at about 260 °C. According to previous works [14,15] both MgH_2 and Mg_2FeH_6 phases were also present in this kind of samples as well as in the 2Mg–Fe material after cycling. Varin et al. [11] observed that the MgH_2–Mg_2FeH_6 hydride mixture synthesized by RMM decomposes in a single endothermic event. They also noticed that well-defined, narrow peaks indicate the presence of small and well crystallized hydride particles, providing homogeneous phase composition, bulk hydrogen distribution and particle size distributions [11].

In order to calculate the ratio of hydride phases for the 2Mg–Fe material, DSC curves were measured at slower heating rate of 1 °C/min in which it was possible to distinguish two thermal events belonging to MgH_2 and Mg_2FeH_6 decomposition [19]. The MgH_2 to Mg_2FeH_6 ratio for the 2Mg–Fe material calculated by DSC and XRD shows a decrease about 60% after cycling.

In Fig. 3A and B, SEM micrographs of 2Mg–Fe after cycling conditions are shown. Agglomerate sizes of the material are in the range from 10 μm to 100 μm and it presents surfaces with irregular shapes. In Table 1, it can be noticed that the crystallite sizes as well as the average agglomerate sizes of 2Mg–Fe cycled sample are larger than that of the non-cycled one.

Fig. 2C, D, E and F show the XRD patterns and DSC curves of the 3Mg–Fe and 15Mg–Fe before and after cycling. In the XRD patterns of non-cycled samples, MgH_2 and Fe are detected. In the case of non-cycled 15Mg–Fe, it is also noticed the presence of metastable γ-MgH_2 and a small amount of MgO. Metastable γ-MgH_2 appears due to the structural defects and the mechanical deformation that occur during the RMM processing [32]. The presence of small amounts of MgO can be attributed to a larger surface area of free Mg generated by the milling process, the large proportion of Mg particles which are not coated with Fe and the high reactivity of Mg to oxygen [8,31]. After cycling, the XRD patterns of both materials show reflections of the MgH_2, Mg_2FeH_6, Fe, Mg, and traces of MgO and $Mg(OH)_2$ phases (Fig. 2C(b) and E(b)). The small amount of the last two phases might have been formed during storage inside the glove box.

In Fig. 2D the DSC curves of the 3Mg–Fe material before and after cycling are compared. For the non-cycled 3Mg–Fe, the endothermic event corresponds to the MgH_2 decomposition. In the case of 3Mg–Fe cycled, and considering the corresponding XRD pattern, the thermal event includes the MgH_2 and Mg_2FeH_6 decompositions. In the DSC curve of 3Mg–Fe cycled there is a noticeable peak maximum at about 275 °C followed by a slight shoulder at about 300 °C, related to the MgH_2 and Mg_2FeH_6 overlapped decompositions, respectively. This observation is supported by DSC curves practiced at slower heating rates of 1 °C/min and 2 °C/min (curves not shown) in which is possible to distinguish the two thermal events associated with MgH_2 and Mg_2FeH_6 decompositions [19]. The DSC curve of non-cycled 15Mg–Fe (Fig. 2F(a)) presents a non-symmetrical form. This shape is due to the lower decomposition temperature of the metastable γ-MgH_2 followed by the stable MgH_2 (β phase) decomposition [8,31,32].

After cycling (Fig. 2F(b)), 15Mg–Fe decomposes in a single endothermic event which seems to be almost in the same temperature range of β-MgH_2 decomposition. In comparison to the non-cycled materials, the peak areas of the cycled materials are smaller indicating a decrease in the hydrogen storage capacity after cycling. This is in agreement with the decreasing behavior of the hydrogen storage capacity observed in the cycling experiment (Fig. 1). As seen in Table 1, the hydride phase ratio calculated by DSC and XRD for the 3Mg–Fe is noticeably higher than for the 2Mg–Fe. For the 15Mg–Fe, it was only possible to calculate the relative hydride phase ratio by XRD. This material has the highest hydride phase ratio, indicating that MgH_2 is the main hydride phase after cycling.

Fig. 3 presents SEM micrographs of the agglomerate distribution and surfaces of the 3Mg–Fe (Fig. 3C and D) and

Please cite this article in press as: Puszkiel JA, et al., Hydrogen cycling properties of xMg–Fe materials (x: 2, 3 and 15) produced by reactive ball milling, International Journal of Hydrogen Energy (2015), http://dx.doi.org/10.1016/j.ijhydene.2015.10.140

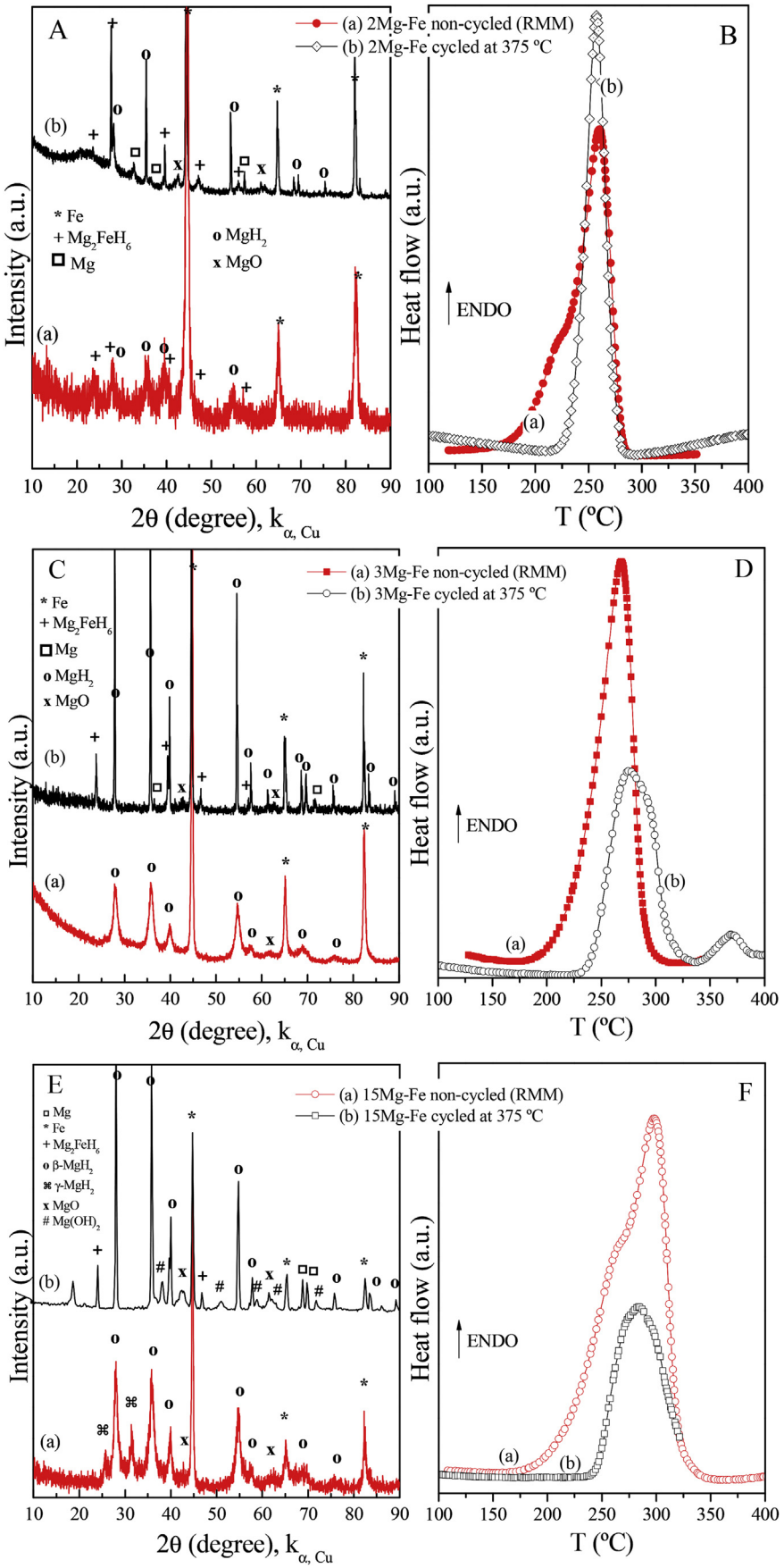

Fig. 2 – XRD and DSC of the (A)–(B) 2Mg–Fe, (C)–(D) 3Mg–Fe and (E)–(F) 15Mg–Fe before and after cycling.

Please cite this article in press as: Puszkiel JA, et al., Hydrogen cycling properties of xMg–Fe materials (x: 2, 3 and 15) produced by reactive ball milling, International Journal of Hydrogen Energy (2015), http://dx.doi.org/10.1016/j.ijhydene.2015.10.140

15Mg–Fe (Fig. 3 E and F) samples after cycling. Both 3Mg–Fe and 15Mg–Fe cycled samples show surfaces with irregular shapes (Fig. 3 D and F). The observed agglomerate sizes for 3Mg–Fe (Fig. 3C), as well as for 2Mg–Fe (Fig. 3A), are in the range from 10 μm to about 100 μm. The average agglomerate size and crystallite sizes of the 3Mg–Fe cycled material are larger than that of the non-cycled (Table 1). For 15Mg–Fe the agglomerates are thinner and their sizes are in the range between 5 μm and 50 μm (Fig. 3E). The 15Mg–Fe after cycling exhibits a larger crystallite size of MgH_2 and the crystallite size of Fe remains in the same value (Table 1). Nonetheless, the average agglomerate size of 15Mg–Fe after cycling is smaller in comparison with the non-cycled 15Mg–Fe.

Discussion

Effect of hydrogen cycling upon the storage capacity

There are several works devoted to the study of the cycling stability of pure Mg/MgH_2 and Mg/MgH_2 plus additives such as transition metals or transition metal compounds (Ni, V, Fe, Ti, Al and Cr_2O_3) [20–25,33–37]. In general, Mg–Fe mixtures were found to be very stable against cycling. In most cases, no capacity loss was observed, in particular when the cycling process was performed at a very high pressure range (around 100 bar) that might have prevented Mg loss due to evaporation. However, hydrogen capacity loss upon cycling was measured in some cases [21,22,34,36,37]. In particular, the capacity loss was detected when samples contained a low amount of Fe (for example, 40 Mg–Fe). In such cases, only a small amount of complex hydride is formed upon hydrogenation. Under such conditions, the authors attributed the observed capacity loss to the agglomeration of Mg particles (associated with the high vapor pressure of Mg and low melting point [21]), segregation of the additives and the formation of stable undesired phases such as MgO or $Mg(OH)_2$.

In this work, a significant mass loss between 20 and 30 mg was measured in all cases after cycling. This mass loss process is associated with the conditions selected for the cycling experiments: 375 °C and from 3000 kPa (absorption) to 300 kPa (desorption). The relatively low desorption pressure can be

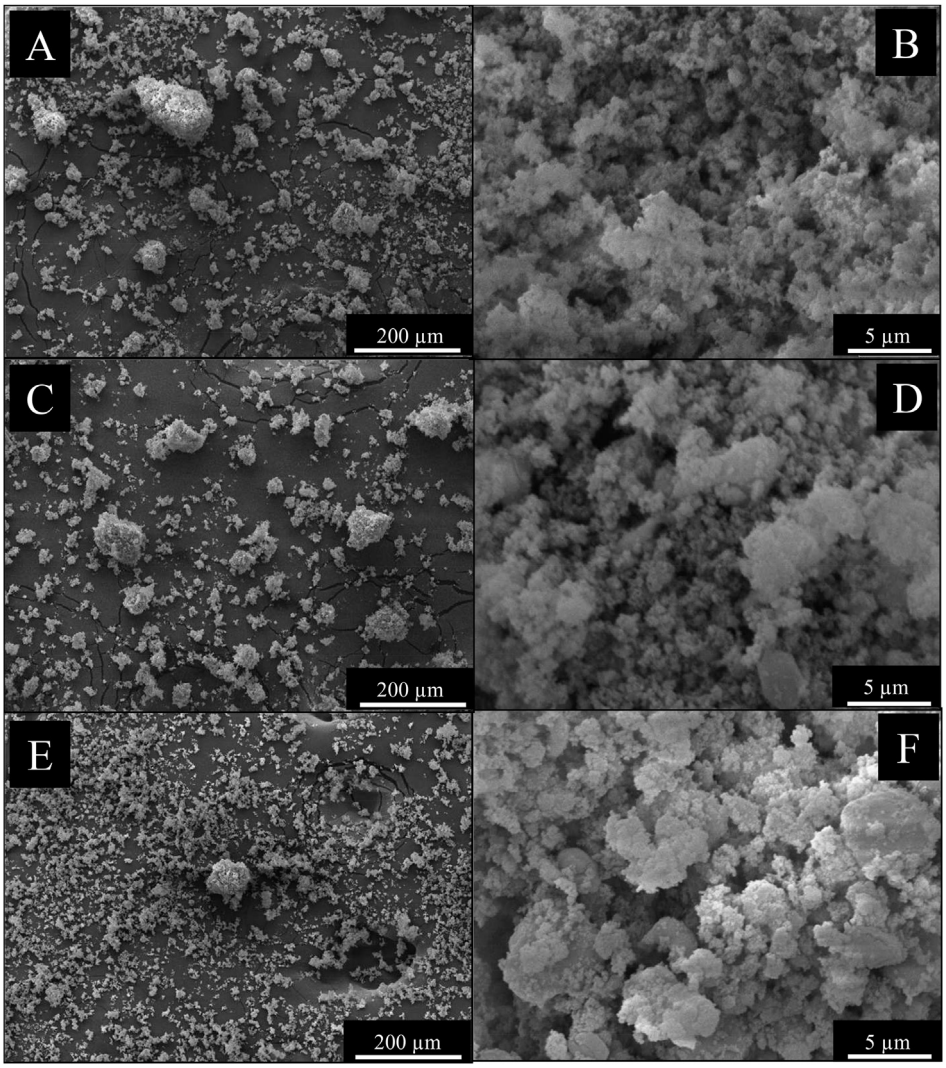

Fig. 3 – SEM micrographs of the xMg–Fe (x: 2, 3 and 15) materials after cycling. A and B: 2Mg–Fe. C and D: 3Mg–Fe. E and F: 15Mg–Fe.

Please cite this article in press as: Puszkiel JA, et al., Hydrogen cycling properties of xMg–Fe materials (x: 2, 3 and 15) produced by reactive ball milling, International Journal of Hydrogen Energy (2015), http://dx.doi.org/10.1016/j.ijhydene.2015.10.140

Table 1 – Characterization of the xMg–Fe materials (x: 2, 3 and 15) after synthesis (non-cycled) and cycling at 375 °C: Ratio of hydride phases calculated from the DSC curves and the XRD diffractograms via the K method [28]. Crystallite size calculated by Scherrer method [27]: MgH_2 (2θ: 27.9°, [110]), Mg_2FeH_6 (2θ: 24.1°, [111]) and Fe (2θ: 44.5°, [111]). Mean agglomerate size of the materials after synthesis and cycling.

Sample	DSC	XRD				PSD
	Ratio between the relative amount of hydride phases [X MgH_2/X Mg_2FeH_6]	Ratio between the relative amount of hydride phases [X MgH_2/X Mg_2FeH_6]	Crystallite size (nm)			Mean volume agglomerate size (μm)
			MgH_2	Mg_2FeH_6	Fe	
2Mg–Fe/H_2 non-cycled[c]	0.8	1.65	10	10	20	20[a]
2Mg–Fe/H_2 cycled at 375 °C	0.5	1.10	20	–	30	30[a,b]
3Mg–Fe/H_2 non-cycled[c]	–	–	10	–	30	25[a]
3Mg–Fe/H_2 cycled at 375 °C	4.5	5.80	65	35	50	40[a,b]
15Mg–Fe/H_2 non-cycled	–	–	10	–	30	25[a]
15Mg–Fe/H_2 cycled at 375 °C[c]	–	7.20	30	30	30	10[a,b]

[a] Mean agglomerate sizes taken from SEM micrographs of sticker mounted samples.
[b] Mean volume agglomerate size determined by particle size distribution analyzer.
[c] The relative amounts of phases were not calculated by DSC because it was not possible to observe two thermal events, even at slower heating rates.

responsible of Mg evaporation. Moreover, under these mild conditions the Mg_2FeH_6 complex hydride is not fully cycled. At this point, it is worth remembering that these cycling conditions were chosen in order to study the behavior of the system under less-severe situations, closer to a possible practical application of these materials.

Table 2 shows a comparison between the measured and calculated hydrogen capacities of the extreme compositions: 2Mg–Fe and 15Mg–Fe. Additionally, the calculated relative amounts of phases and the MgH_2/Mg_2FeH_6 ratios from XRD patterns (Fig. 2 A and E) are shown. The hydrogen capacities and relative amount of phases were determined taking into account the MgH_2/Mg_2FeH_6 ratios from XRD patterns and assuming that the sample mass loss during cycling is due to active Mg evaporation. In Fig. 2A, C and E, the XRD patterns before and after cycling show the presence of free Mg. However, the low intensity of the XRD peaks of free Mg suggests that for the calculations the free Mg can be neglected owing to its low amounts, in accordance with the mass loss assumption.

As seen in Table 2, the measured and calculated hydrogen capacities are in good agreement. In most cases, both hydrides MgH_2 and Mg_2FeH_6 are detected (Fig. 2A, C, E). For both 2Mg–Fe and 15Mg–Fe materials, the amount of MgH_2 decreases after cycling (Tables 1 and 2). In the case of the 2Mg–Fe material, the amount of Mg_2FeH_6 is slightly larger after cycling (Table 2). It suggests that Mg_2FeH_6 is formed and then remains stable. The 15Mg–Fe material does not contain Mg_2FeH_6 before cycling. However, it has 11% of Mg_2FeH_6 after cycling (Table 2).

Based on the results and the analysis, the hydrogen capacity loss during cycling is ascribed to two effects: 1 – the evaporation of the active fraction of Mg which causes the mass loss and 2 – the formation of Mg_2FeH_6 complex hydride upon hydrogenation which remains stable because its equilibrium pressure at 375 °C (about 500 kPa [8]) is near to the used dehydrogenation pressure (300–250 kPa).

Effect of hydrogen cycling upon the hydrogen kinetic behavior

Hydrogenation kinetic behavior

In our previous works [15,19], we found that under dynamic conditions Mg_2FeH_6 is mainly formed at temperatures above 350 °C. When the temperature is 375 °C, the pressure necessary to form the complex hydride must be above 1500 kPa [19]. The formation of Mg_2FeH_6 under dynamic conditions involves a two-step reaction with MgH_2 as an intermediate phase and the subsequent formation of Mg_2FeH_6 from the reaction between MgH_2 and Fe particles. This MgH_2 and Fe particles interaction is enhanced by higher temperatures since it involves solid–solid diffusion mechanism. In addition, this solid–solid diffusion effect also constraints the full conversion under cycling to Mg_2FeH_6, leading to the MgH_2–Mg_2FeH_6 hydride mixture formation [19]. It was also observed that the formation of Mg_2FeH_6 slows down the overall hydrogenation

Table 2 – Comparison between the measured hydrogen capacities and calculated hydrogen capacities with their relative amount of phases before and after cycling for 2Mg–Fe and 15Mg–Fe.

Sample	Hydrogen capacity (wt.%)		Calculated relative amount of phases (wt.%)				Ratio between the relative amount of hydride phases [X MgH_2/X Mg_2FeH_6] XRD
	Measured	Calculated	MgH_2	Mg_2FeH_6	Fe	Mg	
2Mg–Fe non-cycled	2.8	2.9	37	23	40	0	1.6
2Mg–Fe cycled at 375 °C	2.2	2.2	30	27	43	0	1.1
15Mg–Fe non-cycled	6.6	6.7	88	0	12	0	–
15Mg–Fe cycled at 375 °C	4.3	5.2	80	11	9	0	7.2

Please cite this article in press as: Puszkiel JA, et al., Hydrogen cycling properties of xMg–Fe materials (x: 2, 3 and 15) produced by reactive ball milling, International Journal of Hydrogen Energy (2015), http://dx.doi.org/10.1016/j.ijhydene.2015.10.140

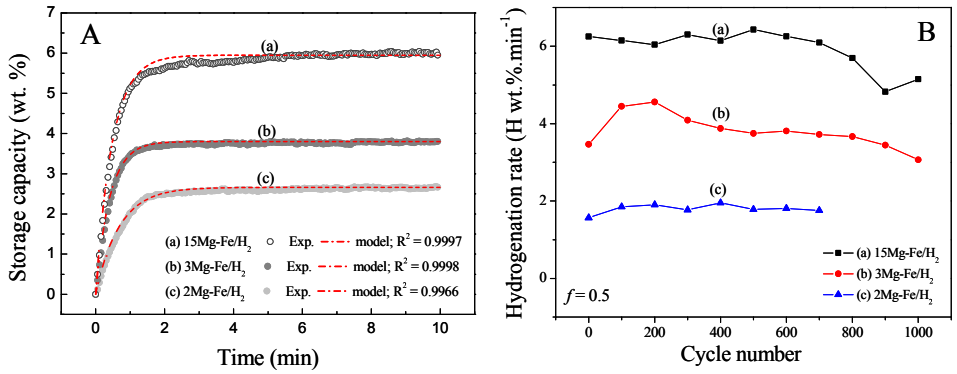

Fig. 4 – A – Hydrogenation kinetic behavior at cycle 200 for xMg–Fe (x = 2, 3, 15) and fitting of the JMA model with n = 1.08. B – Hydrogenation rate at $f = 0.5$ obtained from each fitted expression against the number of cycles for xMg–Fe at 375 °C (x = 2, 3, 15).

rate owing to the solid–solid diffusion effect [15,19]. Thus, at temperatures above 350 °C the hydrogenation rate is slower than that observed at lower temperatures. The hydrogenation process at low temperatures (<350 °C) just results in the faster formation of MgH_2 catalyzed by Fe because the solid–solid diffusion effect is totally hindered precluding the Mg_2FeH_6 formation.

In Fig. 4 the hydrogenation kinetic behavior at the cycle 200 (Fig. 4A) and the hydrogenation rates as a function of the number of cycles (Fig. 4B) for all the compositions are shown. The analysis of the hydrogenation mechanism for the curves at 200 cycles was done by fitting the JMA equation as a function of the hydrogen storage capacity against time (Fig. 4A, dash lines) and by applying the integral form of the equation against time (figures shown as Supplementary Material: Fig. S1). Moreover, the effect of cycling on the hydrogenation mechanism and hydrogenation rates were evaluated by fitting the JMA equation expressed as reacted fraction by using equation (3). For all cases, i.e. Mg–Fe compositions and hydrogenation processes at different cycle numbers, excellent fitting agreements (correlation coefficient $R^2 \sim 1$) were obtained with the same exponent n = 1.08. It has also been noticed that the fitting agreement is quite sensitive to the actual value of the n exponent. Thus, this exponent can be reasonably taken as $n \cong 1$. Investigations via scanning electron microscopy with partially reacted MgH_2 particles showed shrinking core morphology with continuous Mg–H (solid solution)/MgH_2 interface boundaries during the hydrogenation stage [38]. In addition, the fact that the hydrogen diffusion coefficient in MgH_2 is much smaller than in Mg solid solution supports the shrinking core morphology [39]. This observations suggests that the dimensionality of the hydrogenation mechanism of MgH_2 can be taken as $d = 2$ and the controlling step mechanism as $m = 2$ for a diffusion growth controlled process. Assuming a constant nuclei number (eq. (5)) and considering fast nucleation, the mechanism provided by the obtained $n \cong 1$ is consistent with two dimensional controlled growth in accordance with ref. [29,40].

It is noticed that the hydrogenation kinetic behavior at the cycle 200 and the hydrogenation rates show a correlation with the Mg–Fe composition (Fig. 4). The hydrogenation rates increase as the proportion of Fe decreases (Fig. 4 B). This fact is due to the higher hydrogen capacity reached in similar times as the amount of active Mg increases, i.e. from 2Mg–Fe to 15Mg–Fe (Fig. 4 A). Interestingly, for each composition the hydrogenation mechanism does not change during the entire cycling process and the hydrogenation rate is about constant, suggesting that the cycling process only causes minor changes in the hydrogenation kinetic behavior. Similar results have been obtained by Dehouche et al. [33,35] with MgH_2 plus Cr_2O_3 as additive. They observed that the hydrogenation rate is not affected by cycling, but a detrimental effect was noticed for the dehydrogenation kinetic behavior.

Dehydrogenation kinetic behavior

In order to elucidate the effect of hydrogen cycling upon the dehydrogenation kinetic behavior of the Mg–Fe materials, the dehydrogenation activation energies for the 3Mg–Fe and 15Mg–Fe materials after cycling were calculated by the Kissinger method [30] from DSC curves (figures shown as Supplementary Material: Figs. S2, S3 and S4). The 3Mg–Fe and 15Mg–Fe were selected to this analysis since they are the representative of extreme compositions. On one hand, the 3Mg–Fe composition is nearby 2Mg–Fe but it contains more MgH_2, which is the active hydride phase during cycling. Additionally it is possible to easily characterize the activation energy for both MgH_2 and Mg_2FeH_6 from the DSC results. On the other hand, the 15Mg–Fe practically contains MgH_2. Thus, this analysis allows evaluating the effect of cycling upon a relevant kinetic parameter such as the activation energy over the whole range of investigated compositions. In Table 3 the dehydrogenation activation energies along with the mean agglomerate and crystallite sizes and the ratios of hydride phases are shown.

For the xMg–Fe (x: 3 and 15), both non-cycled and cycled materials present refined microstructures with mean agglomerate sizes below 40 μm and crystallite sizes ranging between 10 nm and 65 nm (Table 1). Dornheim et al. have reported that the influence of the crystallite size on the hydrogen kinetic behavior for MgH_2 is more obvious when the

Please cite this article in press as: Puszkiel JA, et al., Hydrogen cycling properties of xMg–Fe materials (x: 2, 3 and 15) produced by reactive ball milling, International Journal of Hydrogen Energy (2015), http://dx.doi.org/10.1016/j.ijhydene.2015.10.140

Table 3 – Activation energies for MgH_2 and Mg_2FeH_6 dehydrogenation. Mean agglomerate size and crystallite size: MgH_2 (20: 27.9°, [110]), Mg_2FeH_6 (20: 24.1°, [111]). Ratio of relative amounts of hydride phases calculated from the DSC measurements and the XRD diffractograms. Materials after hydrogen cycling at 375 °C: 3Mg–Fe and 15Mg–Fe.

Materials	Dehydrogenation E_a [kJ/mol H_2]		Mean volume agglomerate size (μm) PSD	Crystallite size (nm) XRD			Ratio between the relative amount of hydride phases [X MgH_2/X Mg_2FeH_6] XRD
	MgH_2	Mg_2FeH_6		MgH_2	Mg_2FeH_6	Fe	
3Mg–Fe/H_2 cycled at 375 °C	113 ± 9	106 ± 8	40	65	35	50	5.80
15Mg–Fe/H_2 cycled at 375 °C	113 ± 1		10	30	30	30	7.20

particle size is larger than 0.7 μm [41]. Furthermore, the kinetic behavior of MgH_2 deteriorates substantially when the crystallite size is larger than 80 nm. During cycling of xMg–Fe (x: 2, 3 and 15) materials, MgH_2 is the main cycled phase and it presents small crystallite sizes (Table 1). Moreover, the mean agglomerate sizes of these materials do not significantly change after cycling. Hence, a degradation of the dehydrogenation kinetic behavior due to deterioration of the microstructure of the materials upon cycling can be discarded. It is noticed that for all xMg–Fe (x: 2, 3 and 15) compositions, the DSC decomposition peaks occur at higher temperatures for the cycled materials than for the corresponding non-cycled materials (see Fig. 2B, D and F). The fact that the decomposition temperatures measured by means of DSC are higher than for the non-cycled material might be attributed to the presence of MgO [11,12].

We found that the dehydrogenation mechanism of the MgH_2–Mg_2FeH_6 hydride mixture proceeds in two independent steps: first MgH_2 decomposes and then the decomposition of Mg_2FeH_6 occurs. The first step can actually activate the latter one, and the presence of Mg_2FeH_6 can improve the dehydrogenation characteristics of MgH_2. This mechanism is due to synergetic-destabilizing effects as a result of hydride phase interactions. On one hand, the presence of both hydrides results in a material with improved microstructural characteristics leading to a mutual interaction during dehydrogenation, i.e. contraction – strain mechanisms acting as decomposition activators. On the other hand, destabilizing effects can lower the decomposition activation energy, Ea [19]. Nonetheless, during cycling the Mg_2FeH_6 is not active and the quantity of Mg_2FeH_6 formed during cycling is also reduced. Thus, there is no beneficial effect of the Mg_2FeH_6 upon the dehydrogenation kinetic during cycling.

The 3Mg–Fe and 15Mg–Fe cycled materials present practically the same dehydrogenation E_a of 113 kJ/mol H_2 for MgH_2 active hydride phase (Figs. S2 and S4, Table 3). For the Mg_2FeH_6 inactive hydride phase, the dehydrogenation E_a has a value of 106 ± 8 kJ/mol H_2 which is in agreement with the value reported for this complex hydride in a MgH_2–Mg_2FeH_6 hydride mixture without cycling, i.e. 104 ± 2 kJ/mol H_2 [19]. Thus, it also indicates that the Mg_2FeH_6 does not take part during the cycling process.

Considering the MgH_2 active hydride phase, the dehydrogenation E_a = (69 ± 7) kJ/mol H_2 (Fig. S3, Table 3) corresponding to 15Mg–Fe after 110 cycles is noticeably lower than that of the samples after cycling of (E_a = (113 ± 1) kJ/mol H_2) [31]. Therefore, the cycling process has a detrimental effect on the dehydrogenation kinetic properties of the MgH_2 active hydride phase. This deterioration can be mainly attributed to the fact that Mg_2FeH_6 is present in a small amount and does not take part in the dehydrogenation process, precluding the previously observed dehydrogenation synergetic effect owing to MgH_2 and Mg_2FeH_6 simultaneous decomposition [19].

Conclusions

The hydrogen cycling characteristics of xMg–Fe (x = 2, 3 and 15) materials prepared via RMM were investigated at 375 °C in the 250 kPa–3000 kPa pressure range. It was found that active

Please cite this article in press as: Puszkiel JA, et al., Hydrogen cycling properties of xMg–Fe materials (x: 2, 3 and 15) produced by reactive ball milling, International Journal of Hydrogen Energy (2015), http://dx.doi.org/10.1016/j.ijhydene.2015.10.140

hydride phase upon cycling is MgH_2. An analysis of the results leads to the conclusion that the hydrogen capacity reduction during cycling can be attributed to two combined effects: 1 – Mg evaporation due to the mild pressure conditions and 2 – the formation of stable Mg_2FeH_6 owing to the dehydrogenation pressure condition. The influence of cycling upon the hydrogen kinetic behavior was also analyzed. The cycling process does not alter the hydrogenation kinetic behavior. However, dehydrogenation kinetic properties of the MgH_2 are deteriorated by cycling. This fact is attributed to the small amount of Mg_2FeH_6 that does not take part in the dehydrogenation process, hindering the dehydrogenation synergetic effect owing to MgH_2 and Mg_2FeH_6 simultaneous decomposition.

Acknowledgments

The authors thank CONICET, ANPCyT (Projects: PICT 2013 (1052) and PICT 2012 (1049)) and Instituto Balseiro (UNCuyo) for partial financial support to carry out this work. The authors also thank F. Castro for the XRD measurements, Jorge Menghini for the PSD measurements, Julio Andrade Gamboa for discussing XRD methods and Department of Characterization of Materials for the SEM and XRD devices and the assistance to perform the SEM observations.

Appendix A. Supplementary data

Supplementary data related to this article can be found at http://dx.doi.org/10.1016/j.ijhydene.2015.10.140.

REFERENCES

[1] Welter J-M, Rudman PS. Iron catalyzed hydriding of magnesium. Scr Metall 1982;16:285–6.
[2] Ivanov E, Konstanchuk I, Stepanov A, Boldyrev V. Magnesium mechanical alloys for hydrogen storage. J Less-Common Met 1987;131:25–9.
[3] Liang G, Huot J, Boily S, Van Neste A, Schulz R. Catalytic effect of transition metals on hydrogen sorption in nanocrystalline ball milled MgH_2 – Tm (Tm=Ti, V, Mn, Fe and Ni) systems. J Alloys Compd 1999;292:247–52.
[4] Bobet J-L, Akiba E, Nakamura Y, Darriet B. Study of Mg-M (M=Co, Ni, Fe) mixture elaborated by reactive mechanical alloying – hydrogen sorption properties. Int J Hydrogen Energy 2000;25:987–96.
[5] Berlouis LEA, Cabrera E, Hall-Barientos E, Hall PJ, Dodd SB, Morris S, et al. Thermal analysis investigation of hydriding properties of nanocrystalline Mg–Ni and Mg–Fe–based alloys prepared by high-energy ball milling. J Mater. Res 2001;16:45–57.
[6] Hanada N, Ichikawa T, Fujii H. Catalytic effect of nanoparticle 3d-transition metals on hydrogen storage properties in magnesium hydride MgH_2 prepared by mechanical milling. J Phys Chem B 2005;109:7188–94.
[7] Bassetti A, Bonetti E, Pasquini L, Montone A, Grbovic J, Vittori Antisari M. Hydrogen desorption from ball milled MgH_2 catalyzed with Fe. Eur Phys J B 2005;43:19–27.
[8] Puszkiel JA, Arneodo Larochette P, Gennari FC. Hydrogen storage properties of Mg_xFe (x: 2, 3 and 15) compounds produced by reactive ball milling. J Power Sources 2009;186:185–93.
[9] Konstanchuk YG, Ivanov E, Pezat M, Darriet B, Boldyrev V, Hagenmuller P. The hydriding properties of a mechanical alloy with composition Mg–25%Fe. J Less-Common Met 1987;131:181–9.
[10] Song-Lin L, Varin RA, Morozova O, Khomenko T. Controlled mechano-chemical synthesis of nanostructured ternary complex hydride Mg_2FeH_6 under low-energy impact mode with and without pre-milling. J Alloys Compd 2004;384:231–48.
[11] Varin RA, Li S, Wronski Z, Morozova O, Khomenko T. The effect of sequential and continuous high-energy impact mode on the mechano-chemical synthesis of nanostructured complex hydride Mg_2FeH_6. J Alloys Compd 2005;390:282–96.
[12] Varin RA, Li S, Chiu Ch, Guo L, Morozova O, Khomenko T, et al. Nanocrystalline and non-crystalline hydrides synthesized by controlled reactive mechanical alloying/milling of Mg and Mg–X (X = Fe, Co, Mn, B) systems. J Alloys Compd 2005;404–406:494–8.
[13] Zhou DW, Li SL, Varin RA, Peng P, Liu JS, Yang F. Mechanical alloying and electronic simulations of 2Mg–Fe mixture powders for hydrogen storage. Mater Sci Eng A 2006;427:306–15.
[14] Puszkiel JA, Arneodo Larochette P, Gennari FC. Thermodynamic and kinetic studies of Mg–Fe–H after mechanical milling followed by sintering. J Alloys Comp 2008;463:134–42.
[15] Puszkiel JA, Arneodo Larochette P, Gennari FC. Thermodynamic-kinetic characterization of the synthesized Mg_2FeH_6–MgH_2 hydrides mixture. Int J Hydrogen Energy 2008;33:3555–60.
[16] Song-lin L, Sheng-Long T, Yi L, Shu-ke P, Jian-Min C. Synthesis of nanostructured Mg_2FeH_6 hydride and hydrogen sorption properties of complex. Trans Nonferrous Met. Soc China 2010;20:2281–8.
[17] Asselli AAC, Jorge Jr AM, Ishikawa TT, Botta WJ. Mg_2FeH_6-based nanocomposites with high capacity of hydrogen storage processed by reactive milling. Mat Res 2012;15(2):229–35.
[18] Asselli AAC, Leiva DR, Jorge Jr AM, Ishikawa TT, Botta WJ. Synthesis and hydrogen sorption properties of MgH_2–Mg_2FeH_6 nanocomposites prepared by reactive milling. J Alloys Compd 2012;5365:S250–4.
[19] Puszkiel JA, Gennari FC, Arneodo Larochette P, Karimi F, Pistidda C, Gosalawit-Utke R, et al. Sorption behavior of the MgH_2-Mg_2FeH_6 hydride storage system synthesized by mechanical milling followed by sintering. Int J Hydrogen Energy 2013;38:14618–30.
[20] Reiser A, Bodanovič B, Schlichte K. The application of Mg-based metal-hydrides as heat energy storage system. Int J Hydrogen Energy 2000;25:425–30.
[21] Bodanovič B, Reiser A, Schlichte K, Spliethoff B, Tesche B. Thermodynamics and dynamics of the Mg–Fe–H system and its potential for thermochemical thermal energy storage. J Alloys Compd 2002;345:77–89.
[22] Feldehoff M, Bogdanovič B. High temperature metal hydrides as heat storage materials for solar and related applications. Int J Mol Sci 2009;10:325–44.
[23] Zahiri B, Harrower CT, Amirkhiz BS, Mitlin D. Rapid reversible hydrogen sorption in Mg-Fe-Ti thin films. Appl Phys Lett 2009;95:103114–23.
[24] Zahiri B, Amirkhiz BS, Danale M, Mitlin D. Bimetallic Fe-V catalyzed magnesium films exhibiting rapid and cyclable hydrogenation at 200 °C. Appl Phys Lett 2010;96. 013108-3.

Please cite this article in press as: Puszkiel JA, et al., Hydrogen cycling properties of xMg–Fe materials (x: 2, 3 and 15) produced by reactive ball milling, International Journal of Hydrogen Energy (2015), http://dx.doi.org/10.1016/j.ijhydene.2015.10.140

[25] Kalisvaart WP, Harrower CT, Haagsma J, Zahiri B, Luber EJ, Ophus C, et al. Hydrogen storage in binary and ternary Mg-based alloys: a comprehensive experimental study. Int J Hydrogen Energy 2010;35:2091–103.
[26] Meyer G, Arneodo Larochette P, Baruj A, Castro FJ, Lacharmoise P, Zacur E, et al. Equipment for hydrogen absorption-desorption cycling characterization of hydride forming materials. Rev Sci Instrum 2007;78. 023903-6.
[27] Alexander L, Klug PH. Determination of crystallite size with the X-ray spectrometer. J Appl Phys 1950;21:137–42.
[28] Zevin Lev S, Kimmel G. Quantitative X-ray diffractometry. New York: Springer; 1995.
[29] Christian JW. The theory of transformations in metals and alloys. 3rd ed. Amsterdam: Pergamon; 2002.
[30] Kissinger HE. Reaction kinetics in differential thermal analysis. Anal Chem 1957;29:1702–6.
[31] Puszkiel JA. Preparation, study and optimization of complex hydrides for hydrogen storage (PhD thesis). Universidad Nacional de Cuyo, Instituto Balseiro; 2012. http://ricabib.cab.cnea.gov.ar/328/.
[32] Gennari FC, Castro FJ, Urretavizcaya G. Hydrogen desorption behavior from magensium hydrides synthesized by reactive mechanical alloying. J Alloys Compd 2001;2001:46–53.
[33] Dehouche Z, Djaozandry R, Huot J, Boily S, Goyette J, Bose TK, et al. Influence of cycling on the thermodynamic and structure properties of nanocrystalline magnesium based hydride. J Alloys Compd 2000;305:264–71.
[34] Bouaricha S, Huot J, Guay D, Schulz R. Reactivity during cycling of nanocrystalline Mg-based hydrogen storage compounds. Int J Hydrogen Energy 2002;27:909–13.
[35] Dehouche Z, Klassen T, Oelerich W, Goyette J, Bose TK, Schulz R. Cycling and thermal stability of nanostructured MgH_2–Cr_2O_3 composite for hydrogen storage. J Alloys Compd 2002;305:319–23.
[36] Zlotea C, Sahlberg M, Oezbilen S, Moretto P, Andersson Y. Hydrogen desorption studies of the $Mg_{24}Y_5$–H system: formation of Mg tubes, kinetics and cycling effects. Acta Mater 2008;56:2421–8.
[37] Polanski M, Bystrzycki J, Varin RA, Plocinski T, Pisarek M. The effect of chromium (III) oxide (Cr_2O_3) nanopowder on the microstructure and cyclic hydrogen storage behavior of magnesium hydride (MgH_2). J Alloys Compd 2011;509:2386–91.
[38] Vigeholm B, Koller J, Larsen B, Pedersen AS. In: Veziroglu TN, Taylor JB, editors. Hydrogen energy progress, vol. V. Oxford: Pergamon; 1984. p. 1455.
[39] Čermák J, Král L. Hydrogen diffusion in Mg-H and Mg-Ni-H alloys. Acta Mater 2008;56:2677–86.
[40] Fernández JF, Sánchez CR. Rate determining step in the absorption and desorption of hydrogen by magnesium. J Alloys Compd 2002;340:189–98.
[41] Dornheim M, Eigen N, Barkhordarian G, Klassen T, Bormann R. Tailoring hydrogen storage materials towards application. Adv Eng Mater 2006;8:377–85.

Please cite this article in press as: Puszkiel JA, et al., Hydrogen cycling properties of xMg–Fe materials (x: 2, 3 and 15) produced by reactive ball milling, International Journal of Hydrogen Energy (2015), http://dx.doi.org/10.1016/j.ijhydene.2015.10.140